

NEUROSCIENCE

Identification of proliferating neural progenitors in the adult human hippocampus

Ionut Dumitru^{1†}, Marta Paterlini^{1†}, Margherita Zamboni¹,
 Christoph Ziegenhain^{1‡}, Sarantis Giatrellis¹, Rasool Saghaleini²,
 Åsa Björklund², Kanar Alkass³, Mathew Tata^{1§}, Henrik Druid³,
 Rickard Sandberg¹, Jonas Frisén^{1*}

Continuous adult hippocampal neurogenesis is involved in memory formation and mood regulation but is challenging to study in humans. Difficulties finding proliferating progenitor cells called into question whether and how new neurons may be generated. We analyzed the human hippocampus from birth through adulthood by single-nucleus RNA sequencing. We identified all neural progenitor cell stages in early childhood. In adults, using antibodies against the proliferation marker Ki67 and machine learning algorithms, we found proliferating neural progenitor cells. Furthermore, transcriptomic data showed that neural progenitors were localized within the dentate gyrus. The results contribute to understanding neurogenesis in adult humans.

Most studies on human hippocampal neurogenesis have assessed the presence of proteins associated with neurogenesis at different stages from neural stem cells, through intermediate neural progenitor cells (INPs) and neuroblasts (hereafter referred collectively to as neural progenitor cells) to new neurons (1). Several studies have reported immunohistochemical evidence of neural progenitor-associated markers in the human dentate gyrus throughout life (2–8), whereas others report their absence beyond childhood, questioning the existence of adult hippocampal neurogenesis in humans (9–11). Methodological differences likely contribute to these conflicting results (1, 12) and it remains open whether these markers, despite their validation in other species, reliably identify neural progenitors in humans.

Single-nucleus RNA sequencing (snRNA-seq) provides an unbiased investigation of cell types and states, surpassing marker limitations and enabling cross-species and developmental trajectory comparisons (13). Recent snRNA-seq studies of the adult human hippocampus identified immature neurons (14) but failed to identify proliferating progenitor cells (14, 15), suggesting that new neurons arise through slow maturation of neuronal progenitors generated during development (14, 15). Bromodeoxyuridine (BrdU) labeling, carbon dating (16, 17), and mitotic generation of neurons in adult human dentate gyrus explants (14) support the presence of proliferating progenitors in the adult human hippocampus. Nevertheless, proliferating progenitors and a neurogenic cell trajectory remained elusive and a missing link for understanding adult hippocampal neurogenesis in humans.

Characterization of hippocampal neural progenitor cells in childhood

To identify neural progenitors in the human hippocampus, we first focused on young individuals (ages 0 to 5 years); based on previous data,

we expected to find high number of neural progenitors in this population (5, 17). We performed droplet-based snRNA-seq of hippocampal nuclei obtained from six individuals (referred to as the childhood group), obtaining a dataset of 115,861 nuclei (table S1). After sample integration to account for batch and individual effects, we manually annotated major cell types based on marker expression (Fig. 1A and figs. S1 and S2) (17–22).

We selected Louvain clusters containing nuclei expressing genes characteristic of the mouse hippocampal neurogenic lineage (fig. S2) (23). Reintegration of these selected cells revealed two large clusters, one dominated by astrocytes and the other by granule neurons (Fig. 1B). These clusters were connected by a trail of nuclei expressing the cell proliferation marker *MKI67* and/or *EOMES* (Fig. 1C), associated with INPs and neuroblasts (24). RNA velocity analysis indicated a progressive differentiation trajectory from the cells expressing INP markers, through the trail of cells expressing neuroblast markers into the granule neuron cluster (Fig. 1D), indicative of a neurogenic lineage and resembling the RNA velocity pattern of mouse hippocampal neurogenesis (25).

We delineated different cell stages in the neurogenic trajectory by Louvain clustering and marker expression (Fig. 1E and fig. S3). INPs and neuroblasts formed discrete clusters whereas putative neural stem cells were dispersed within the astrocyte cluster and were identified by coexpression of *NESTIN*, *PAX6*, *ASCL1*, *SOX2* and low expression of *S100B*. Putative immature neurons, expressing granule neuron and plasticity markers *PROX1*, *ST8SIA2*, *DCX*, and low *GAD2*, were identified near neuroblasts in the granule neuron cluster (fig. S3).

Diffusion map analysis corroborated a trajectory from neural stem cells, to proliferating INPs, neuroblasts, and granule neurons (Fig. 1, F and G, and figs. S4 and S5) (26). Through differential gene expression analysis, we identified additional genes which have not been thoroughly studied in postnatal neurogenesis but are enriched in human INPs and neuroblasts, such as *EZH2*, or in neuroblasts and immature neurons such as *GLRA2*, *EPHA3*, *KCNH7*, and *SEMA3C* (fig. S6, A to D).

Similarities and differences between neural progenitors in young mice and humans

We integrated the human childhood dataset with a juvenile mouse hippocampus dataset (27). Several cell types were fully overlapping in uniform manifold approximation and projection (UMAP) visualization (e.g., the INPs and neuroblasts) whereas others were not (e.g., the putative neural stem cells and immature neurons), suggesting species-specific nuances in gene expression (Fig. 2A and figs. S7 and S8). Hierarchical clustering showed that INPs and neuroblasts were more similar to their mouse counterparts than to other human cell types, indicating transcriptional similarity between human and mouse neurogenic cells (Fig. 2B and figs. S7 and S8).

We compared the neurogenic trajectories between species by plotting human and mouse neural progenitors and immature neurons in diffusion map space, obtaining a combined neurogenic trajectory in which human cells recapitulate the transition stages characteristic of mouse neurogenesis (Fig. 2, C and D). We assessed the distribution of canonical neurogenic markers along the neurogenic trajectory in humans and mice and found expression in both species. However, their dynamics varied during progression from stem cells to immature neurons. *HES6*—specific to INPs and neuroblasts in mice—was expressed in both stem cells and INPs in the childhood human hippocampus. *EOMES*, specific to INPs in mice, was found in both INPs and neuroblasts in humans (Fig. 2, E to H, and fig. S9).

Enrichment and identification of neural progenitors

To identify neural progenitors in the adolescent and adult human hippocampus, we performed snRNA-seq on whole hippocampi or dentate gyri from 19 individuals in the range of 13 to 78 years old (y.o.). In 12 of these individuals (20 to 78 y.o.), neural progenitors were enriched using flowcytometric sorting (for details, see materials and methods and

¹Department of Cell and Molecular Biology, Karolinska Institutet, Stockholm, Sweden. ²Dept of Biology and Biological Engineering, National Bioinformatics Infrastructure Sweden, Science for Life Laboratory, Chalmers University of Technology, Göteborg, Sweden. ³Department of Oncology-Pathology, Karolinska Institutet, Stockholm, Sweden. ^{*}Corresponding author. Email: jonas.frisen@ki.se. [†]These authors contributed equally to this work. [‡]Present address: Department of Medical Biochemistry and Biophysics, Karolinska Institutet, Stockholm, Sweden. [§]Present address: Cancer Research UK, 2 Redman Place, London, UK.

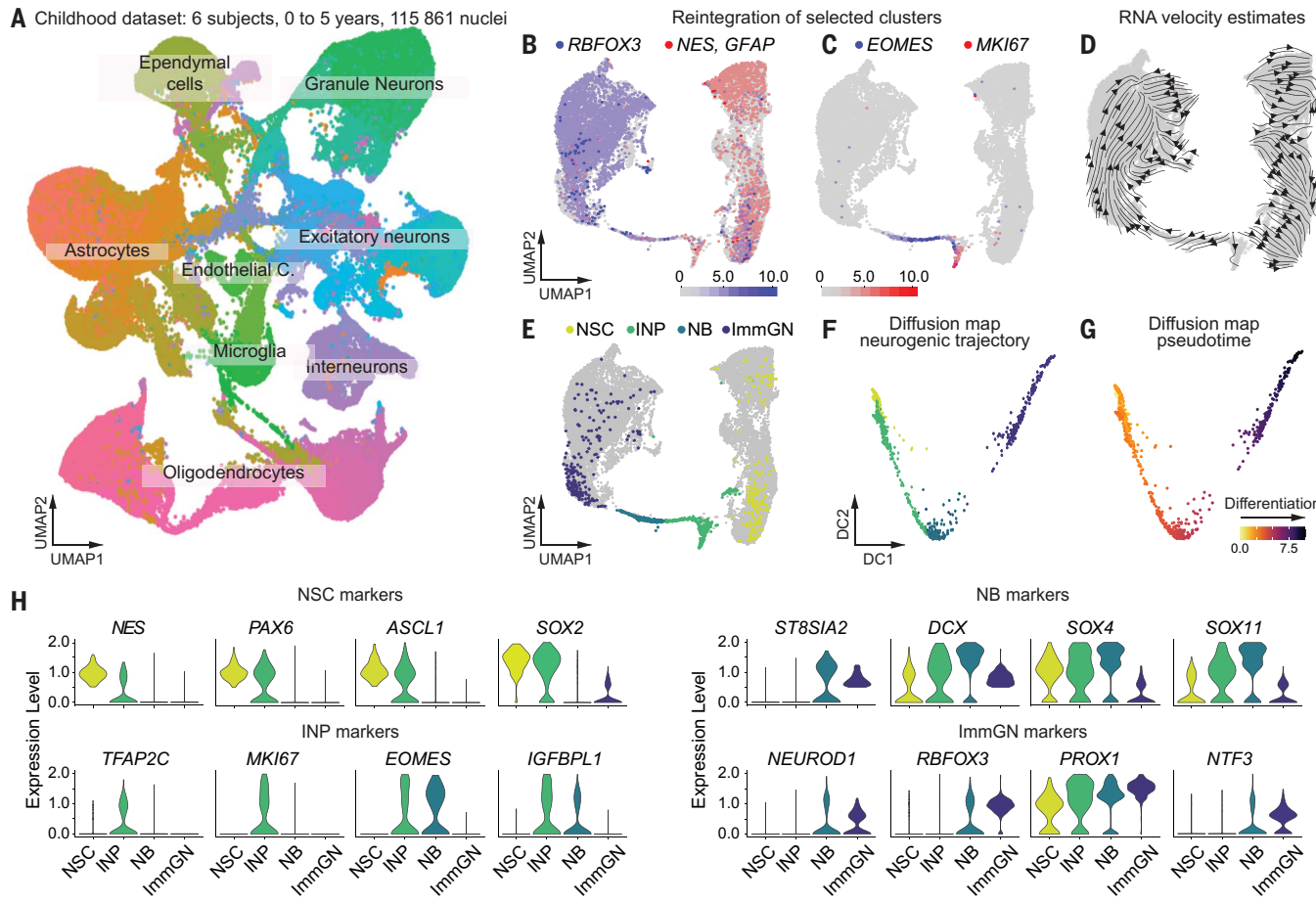


Fig. 1. Delineation of a neurogenic trajectory in the human childhood hippocampus. (A) UMAP projection of the integrated dataset after snRNA-seq of whole hippocampi from individuals ranging from 0 to 5 y.o. (B and C) Clusters coexpressing neurogenic markers were reintegrated. Expression of cluster specific markers projected on the UMAP: (B) *RBFOX3* for neurons and *NES* and *GFAP* for astrocytes/neural stem cells; (C) *EOMES* for INPs and neuroblasts and *MKI67* for dividing cells. (D) RNA velocity estimates derived from the stochastic model projected onto the UMAP-based embedding. (E) Cluster annotation for the reintegrated cells. The separations between astrocytes and neural stem cells (NSC) and between granule neurons (GN) and immature granule neurons (ImmGN) are based on marker expression in which a NSC is defined by *NES*, *ASCL1*, *SOX2*, and *PAX6* expression, whereas an ImmGN is defined by *ST8SIA2*, *DCX*, *PROX1*, and *GLRA2* expression. (F and G) Diffusion map organizing neural stem cells, INPs, neuroblasts, and immature granule neurons in a trajectory that recapitulates their differentiation. (F) Display of how clusters of progenitors are distributed along the trajectory; (G) is a representation of their pseudotemporal ordering. (H) Violin plots displaying gene expression patterns characteristic of NSC, INP, and NB in the clusters obtained after reintegration.

table S1). Of the enrichment protocols tested, the sorting of *Ki67*+ nuclei performed in eight samples proved to be efficient, resulting in a 37-fold enrichment of *MKI67* mRNA-expressing nuclei ($P = 0.018$, Wilcoxon rank sum exact test corrected using the Bonferroni method, fig. S10). Each sorted sample was supplemented with unsorted dentate gyrus cell nuclei from the same donor to enable droplet-based snRNA-seq, yielding 141,021 nuclei (fig. S11). Nuclei from the remaining seven individuals (13 to 31 yo.) were processed without sorting. The final dataset included 286,799 nuclei, leading—after integration with the childhood dataset—to a 402,660-nuclei dataset from individuals ranging in age from 0 to 78 years, in which we identified all major hippocampal cell types through unbiased clustering and manual annotation (fig. S12).

We faced challenges in identifying progenitor cells in the adolescent and adult cohorts when using the same strategy as in the childhood group, and so we instead trained machine learning algorithms (scPred, LMN, and scanVI) (14, 28–30) to identify nuclei transcriptionally similar to childhood INPs and neuroblasts. Nuclei from the adolescent and adult datasets were annotated as progenitors if predicted by at least two algorithms.

The strategy was tested in a juvenile mouse dataset (27), where it identified 83% of the INPs, 49% of the neuroblasts and 91% of all proliferating

progenitors, with only 2 cells misannotated out of 540 cells predicted, indicating a 0.37% false prediction rate (fig. S13). We further applied this analysis strategy to the adult human cortex, in which there is no evidence of postnatal neurogenesis (31, 32). We analyzed 12 cortical datasets (19, 33, 34) with a total of 108,285 nuclei; our strategy predicted one potential progenitor cell, later excluded based on the canonical oligodendrocyte lineage marker expression (fig. S13). Taken together, the data suggest that this strategy conservatively identifies putative neural progenitors with high specificity.

Neural progenitor cells in the adolescent and adult human hippocampus

We applied machine learning to the adolescent and adult hippocampal snRNA-seq dataset and identified a total of 354 progenitor cells (Fig. 3A), which we determined based on their expression patterns and cluster identity to be neural stem cells (12 adolescent, 65 adult), INPs (4 adolescent, 71 adult), and neuroblasts (202 adult) (Fig. 3G). To further characterize the predicted cells and to determine how they compare with neural progenitors of other species, we integrated the whole human dataset generated in this study with published mouse, pig, and rhesus monkey hippocampal snRNA-seq datasets, using the

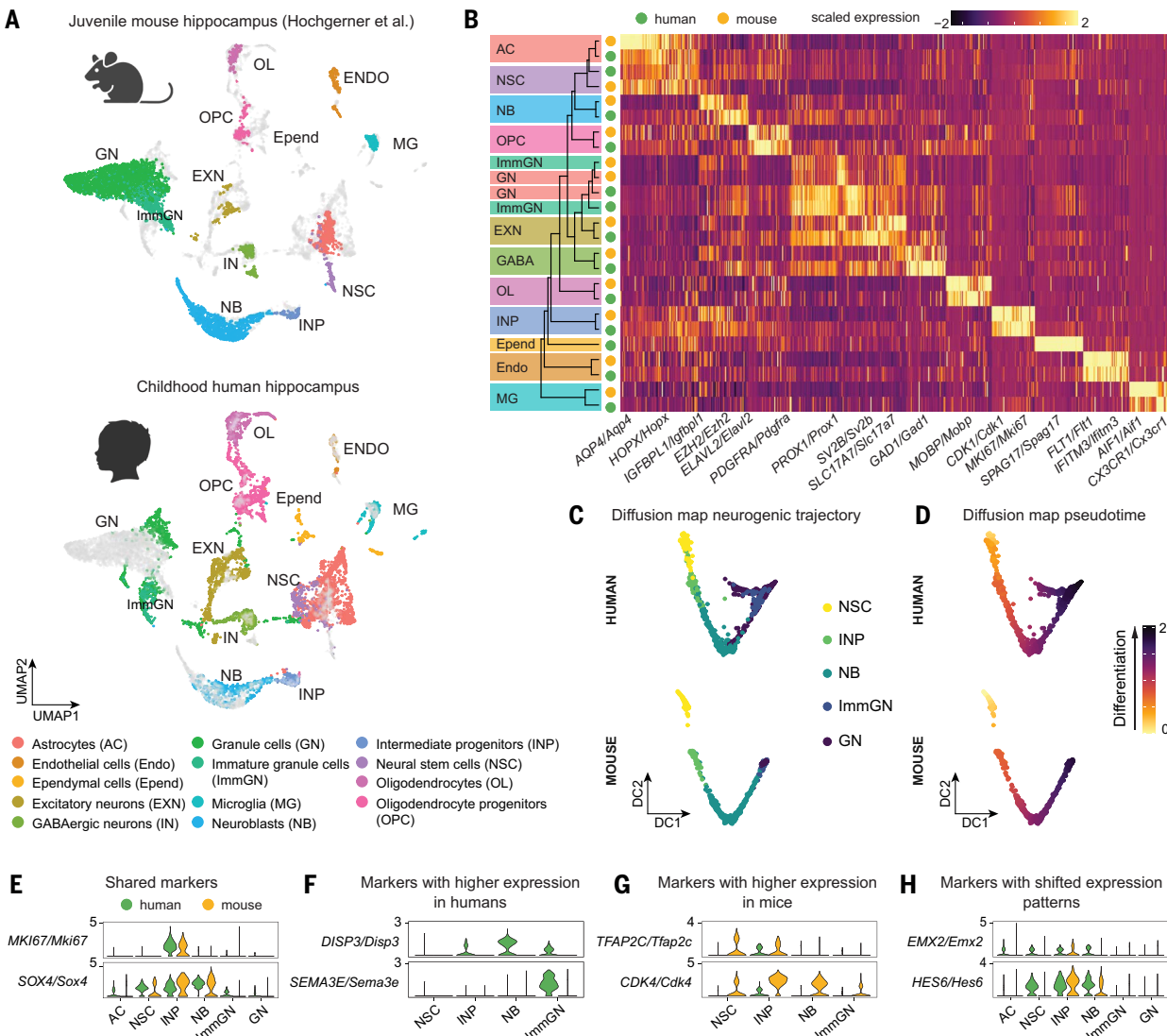


Fig. 2. Comparison of the neural progenitors in the human childhood and juvenile mouse hippocampus. (A) UMAP plots displaying the collection of cell types composing the mouse dentate gyrus and young human dentate gyrus. (B) Heatmap representing the top 50 cell type markers that are conserved across species. Hierarchical clustering on the lefthand side of the plot emphasizes transcriptional similarities of the different cell types between mouse and human. (C and D) Diffusion map organizing the human and mouse neural progenitors from both species in a trajectory that recapitulates their differentiation. (C) shows the cluster distribution along the trajectory, whereas (D) displays the pseudotemporal ordering. (E to H) Violin plots displaying gene expression patterns in mouse and human progenitor cells. They display examples of genes with similar expression (E), enriched in humans (F), enriched in mice (G), or genes that display interspecies differences in the pattern of expression across the neurogenic cells (H).

mouse as reference (15, 27). The human neural progenitors identified in all ages organized along the same neurogenic trajectory as the neural progenitors from the other species (Fig. 3, B to G).

Hierarchical clustering analysis demonstrated that the human adolescent and adult neural stem cells, INPs, and neuroblasts had the highest similarity to the corresponding cell types in the mouse, pig, rhesus monkey, and human childhood datasets (Fig. 3H). We further integrated the human dataset generated in this study with a human fetal hippocampus dataset (35) and the mouse dataset, again using the mouse as a reference (fig. S14) (35). The human neural progenitors identified in this study aligned not only with the mouse progenitors as already described, but also with the human fetal progenitors (fig. S14). This was validated by the hierarchical clustering analysis, which showed that the human childhood and adolescent/adult INPs and neuroblasts were more similar to the corresponding cells in the mouse and human fetal datasets than to any other cell type in the integrated dataset (fig. S14, E to J).

Similar to childhood progenitors, proliferating adolescent and adult progenitors were also enriched in *NES* and *VIM*, likely reflecting their neural stem cell origin, and also show *EZH2*, *SYNE2*, *SYNE1*, *SOX4*, *DRAKIN*, and *HES6* (fig. S15). However, adolescent and adult proliferating progenitors present *EOMES* and *TFAP2C* at low amounts compared with the childhood progenitors, whereas *EZH2*, *SYNE2* and *SOX4* showed similar levels between the two groups (fig. S15 and S16). We found human progenitors to express markers similar to neural progenitors of other species such as those described above, but also genes that appear to be specific to the adult human cells such as *APOLD1* and *RRM2* (fig. S15 and S16). The former gene is expressed in human cortical INPs during development (36), whereas the latter is induced by *ASCL1* expression in INPs (37).

Pseudotemporal analysis (26) in mouse, pig, rhesus monkey, and human nuclei revealed a differentiation trajectory from the neural stem cell cluster, through the INPs and neuroblast clusters and toward the granule neurons with adolescent and adult progenitors distributed along

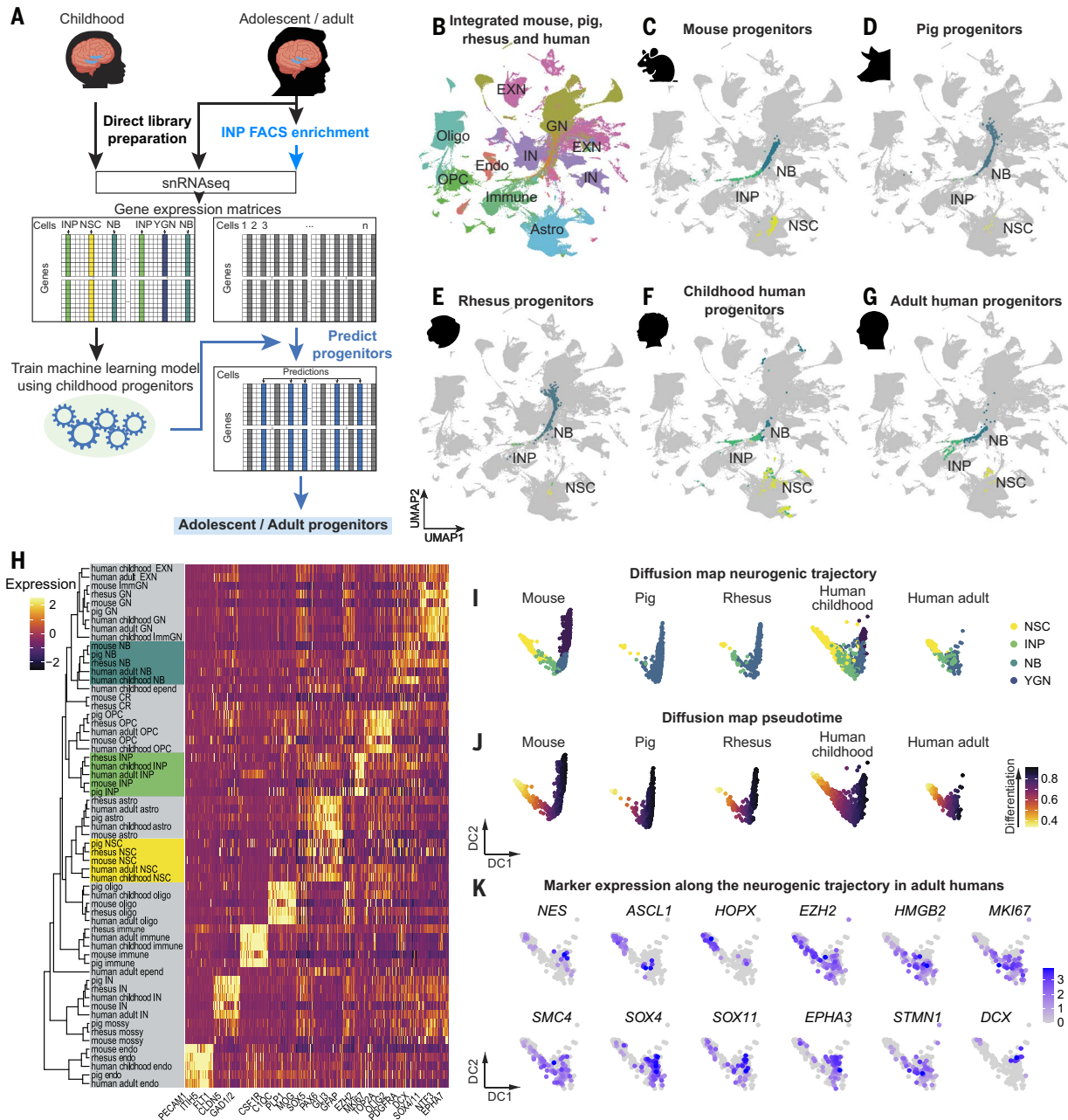


Fig. 3. Neural progenitors in the adult human hippocampus. (A) Scheme depicting the identification of neural progenitors in the adolescent and adult human brain. The transcriptional profiles of the neural progenitors identified in human childhood were used to train machine learning models, which were applied to the adolescent/adult human dataset generated in this study. The adolescent and adult human dataset includes human hippocampi or dentate gyrus samples directly processed to obtain 10x libraries as well as samples subjected to fluorescence-activated cell sorting enrichment for proliferating and/or neural progenitor markers. (B to G) Characterization of the neural progenitors present in the integrated dataset across species. We aligned the human dataset generated in this study with rhesus monkey, pig (15), and mouse data (27), using the latter as a reference for integration. The neural progenitors annotated according to the study of origin are highlighted in the UMAP plot of the integrated dataset: mouse (C), pig (D), rhesus monkey (E), childhood human (F), and adult human (G). (H) Heatmap representing the top 50 cell type markers that are conserved between the mouse, pig, rhesus monkey, childhood, and adolescent/adult human neural progenitors. Hierarchical clustering on the lefthand side of the plot emphasizes the transcriptional similarities of progenitors across species and age groups. (I to K) Diffusion map organizing neural progenitors across species and ages in a continuous trajectory that recapitulates their differentiation. The cluster distribution along the trajectory is presented in (I) and the pseudotemporal ordering in (J). (K) Gene expression patterns of neurogenesis markers along the pseudotemporal ordering of the human adult progenitors as determined with diffusion map.

this route, indicating the presence of a neurogenic trajectory in the adult human hippocampus (Fig. 3, I to K, and fig. S15).

The majority of the neural progenitor cell nuclei in the adolescent and adult dataset were in cell cycle (70% compared with 22% in the childhood dataset). This reflects the flow cytometric enrichment for *Ki67*⁺ nuclei in many samples, and neural progenitors that are not

in cell cycle are selected against in these individuals, resulting in their underrepresentation in relation to the proliferating cells. Almost all INPs were in cell cycle in the adolescent/adult group, regardless of the proliferation marker Ki67 enrichment (table S1). Differential gene expression analysis showed that, similar to childhood proliferating progenitors, the adolescent/adult progenitors in

cell cycle expressed several proliferation markers in addition to *MKI67*, such as *TOP2A*, *CENPF*, *PCNA*, *MCM2*, as well as *SMC4* and *HMGB2* (cell cycle genes described in neural progenitors), corresponding to gene ontology terms related to cell division (fig. S15).

There was substantial interindividual variation in the number of progenitors within the adolescent and adult cohorts (table S1). In the samples that were not enriched for Ki67+ nuclei, adolescents generally had higher numbers compared with adults. However, the highest numbers were seen in some of the adult subjects in whom dentate gyrus nuclei were enriched with antibodies against Ki67 (table S1). Two individuals (40 and 58 yo.) stood out for having much higher numbers of INPs and neuroblasts than other adults. The younger of these two subjects (40 yo.) had a known history of epilepsy, potentially explaining the higher number of progenitor cells (38), whereas the older individual (58 years) had no known pathology. Neural progenitors were identified in all childhood subjects in the group but were absent in 2 out of 4 adolescents and 5 out of the 14 adults (table S1). However, in 6 of the subjects in which we failed to find progenitor cells we could identify immature granule neurons by marker expression (fig. S17 and table S1). One of the samples with no detectable progenitors also had no immature neurons, suggesting both technical as well as biological sources of variation.

Spatial localization of neural progenitor cells in the adult human dentate gyrus

We used RNAscope *in situ* hybridization (39) and Xenium, a spatially resolved transcriptomics platform with single-cell resolution (40), to localize neural progenitor cells in the adult human hippocampus. RNAscope offers very high sensitivity and specificity but allows the analysis of only a few genes simultaneously, limiting the ability to identify cells based on multiple markers. Xenium, on the other hand, allows the multiplexing of hundreds of genes, enabling the identification of major hippocampal cell types through graph-based clustering. Rare cell types do not cluster separately in unsupervised analysis but can be distinguished by their spatial localization in the tissue (for instance, dentate gyrus neural progenitor cells, fig. S18).

In snRNA-seq analysis, identifying progenitor cells based on a small number of marker combinations was challenging. Adding spatial context and narrowing the focus to the granule cell layer of the dentate gyrus and its immediate vicinity partially helped. However, even within this limited region, it is necessary to assess the presence and absence of multiple markers to reliably identify progenitors, which was possible using Xenium (fig. S19). For example, *NES*, *SOX4*, and *SOX11* are expressed by neural progenitors, but other markers are needed as these genes are also expressed by some oligodendrocyte progenitors (*PDGFRα+*, *CSPG4+*) and endothelial cells (*PECAM1+*, *FLT1+*) (fig. S19).

Using Xenium and RNAscope in the dentate gyrus, we identified neural stem cells coexpressing *NESTIN*, *SOX2*, and *ASCL1*, INPs expressing combinations of *ASCL1*, *EOMES*, *SOX2*, *SOX11*, *EZH2*, and *DCX*, and neuroblasts expressing sets of the markers *EZH2*, *EOMES*, *DCX*, *ST8SIA2*, *SOX11*, *IGFBPL1*, *ELAVL4*, *CALB2*, and *STMN1* (Fig. 4 and figs. S19, S20, and S21). We also localized cells expressing the new markers, which we found to be enriched in human neural progenitors such as *EZH2* in proliferating early INPs and in neuroblasts at different maturation stages (fig. S22, A to C and H), and *GLRA2*, *EPHA3*, and *KCNH7* in neuroblasts and/or immature granule neurons, coexpressing *DCX* and/or *CALB2* (fig. S22, D to G). Furthermore, we found that cells expressing combinations of neurogenic and proliferation

markers, without markers of other cell identities, were mostly localized in the dentate gyrus and adjacent hilus region (fig. S23).

DCX has been the most often-used marker to identify neuroblasts and immature neurons in many species, including humans. In snRNA-seq of the whole human hippocampus, *DCX* is broadly expressed and is not in itself informative for identifying neuroblasts (fig. S2F) (12, 14, 41). Within the dentate gyrus granule cell layer, *DCX* expressing cells are very sparse, with 21.8% being *GAD2*-expressing GABAergic interneurons. Of the *DCX*-expressing cells lacking *GAD2*, 22.0% coexpress *CALB2*, associated with more mature neuroblasts (4) ($n = 4$, ages 27 to 53 years, fig. S24). RNAscope for *DCX* and *CALB2* was combined with immunohistochemistry, confirming overlapping gene and protein expression (fig. S25). Using both RNAscope and Xenium, we identified neural stem cells, INPs, and neuroblasts expressing proliferation markers (Fig. 4 and figs. S21 and S26). Proliferating neural stem cells and INPs were often located in pairs or small clusters (Fig. 4 and fig. S22H) and several neuroblasts were often found within a limited area, suggesting ongoing cell division and active neurogenesis. Although several markers were consistently observed (*NES*, *EZH2*, *GLRA2*, *DCX*, or *CALB2*), some were detected less frequently (*EOMES*, *IGFBPL1*, *SOX11*, and *MKI67*), likely reflecting biological heterogeneity. With the enhanced sensitivity of RNAscope and Xenium compared with scRNA-seq, we detected neural progenitors in all 10 cases tested (table S1).

Discussion

We report the identification and molecular characterization of neural progenitor cells from birth through adulthood in the human hippocampus. These cells are more abundant and readily identifiable early in life and become sparser in adolescents and adults. The dentate gyrus is the primary gateway of the hippocampus, controlling how information flows from the cortex to the hippocampus proper. To maintain normal function, granule neurons receive fine-tuned inhibition from local-circuit GABAergic interneurons, with only few responding to activation (42). Immature granule neurons have a period of enhanced

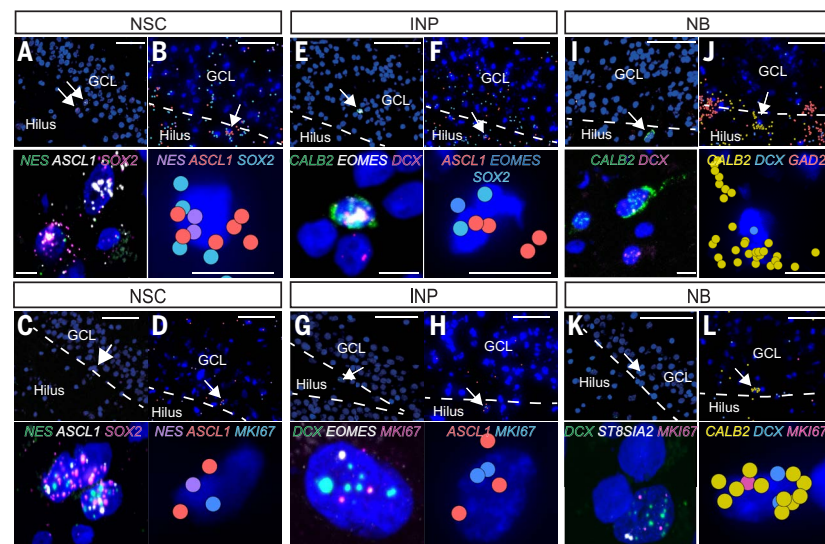


Fig. 4. Single-cell transcriptomic characterization of adult human neural progenitors and of the human neurogenic niches with spatial resolution. (A to D) Example NSCs expressing characteristic markers detected with RNAscope (A) and (C) and Xenium (B) and (D). (E to H) Example INPs expressing characteristic markers detected with RNAscope (E) and (G) and Xenium (F) and (H). (I to L) Example NBs expressing characteristic markers detected with RNAscope (I) and (K) and Xenium (J) and (L). Xenium spatial transcriptomics was performed on brain tissue from a 34-year-old male subject. The cells shown are negative for *PDGFRα*, *CSPG4*, *GAD2*, *ADARB2*, *SOX10*, *MOBP*, *MBP*, *FLT1*, *PECAM1*, and *CD4*. GCL, granular cell layer. Hatched lines indicate the border between the GCL and the hilus. Arrows in the upper panels indicate cells shown in higher magnification in the lower panels.

plasticity when they are highly responsive to excitation, and therefore even a small number of newly generated cells can have a functional impact on the hippocampus (42).

The difficulty in identifying neural progenitors in the human hippocampus has led some to question the existence of neurogenesis. A recent study using snRNA-seq identified and characterized immature granule neurons in the dentate gyrus (14). However, neural stem cells, INPs, and neuroblasts have not been identified in adult humans using unbiased transcriptomics. Our data integrate snRNA-seq with spatially resolved transcriptomics at a single-cell resolution, allowing the identification and visualization of neural progenitors in the adult human hippocampus. It complements the identification of immature granule neurons by capturing and characterizing proliferative neural progenitors, together delineating a full cell trajectory for adult neurogenesis in humans.

The number of nuclei sequenced is critical to the ability to identify very small cell populations, and previous studies have been suggested to be underpowered for identifying neural progenitors (12). Analyzing a large number of subjects and nuclei, specifically isolating nuclei from the dentate gyrus rather than the whole hippocampus, and most importantly enriching for proliferating cells, increased the power to identify rare neural progenitors. Moreover, using machine learning algorithms as previously done by Zhou *et al.* to identify immature neurons (14) was necessary to confidently detect neural progenitor cells in adolescent and adult subjects.

We found that neural progenitor cells in the adult human hippocampus are transcriptionally similar to those in mice, pigs, macaques, and in humans during childhood, with slight species-specific nuances in gene expression, with unclear functional relevance. The identification of a neurogenic cell trajectory with proliferating neural progenitor cells provides a cellular underpinning for the mitotic generation of neurons in the adult human hippocampus, which previously has been demonstrated by BrdU labeling and radiocarbon dating (16, 17). It is unclear whether the generation of immature granule neurons by proliferating progenitors is the main mechanism for adult neurogenesis and to what extent mitotic generation earlier in life and protracted neuronal maturation are complementary pathways.

As expected, the highest number of neural progenitor cells was found in the youngest subjects in the childhood group (5, 17). However, differences in nuclear enrichment protocols make it difficult to draw conclusions about the number of neural progenitor cells at different ages in adulthood. Nevertheless, substantial variation was detected across individuals processed using the same enrichment approaches and variation in the numbers of immature granule neurons was also observed in parallel, consistent with prior reports of variability of neurogenesis among macaques, humans, and inbred mouse strains (12, 14, 17, 41).

Several of the donors had a history of psychiatric or neurological diseases, which have been associated with differences in neurogenesis (2, 3, 42). However, the current study was not powered to draw conclusions about a potential relationship between pathology and neurogenesis. The identification of neural progenitor cells in the adult human brain will facilitate further studies on possible effects of pathology and genetic predisposition on neurogenesis.

REFERENCES AND NOTES

1. G. Kempermann *et al.*, *Cell Stem Cell* **23**, 25–30 (2018).
2. J. Terreros-Roncal *et al.*, *Science* **374**, 6571 (2021).
3. E. P. Moreno-Jiménez *et al.*, *Nat. Med.* **25**, 554–560 (2019).
4. E. P. Moreno-Jiménez, J. Terreros-Roncal, M. Flor-García, A. Rábano, M. Llorens-Martín, *J. Neurosci.* **41**, 2541–2553 (2021).
5. R. Knott *et al.*, *PLOS ONE* **5**, e8809 (2010).
6. M. Boldrini *et al.*, *Cell Stem Cell* **22**, 589–599.e5 (2018).
7. M. K. Tobin *et al.*, *Cell Stem Cell* **24**, 974–982.e3 (2019).
8. A. Ammothumkandy *et al.*, *Nat. Neurosci.* **25**, 493–503 (2022).
9. S. F. Sorrells *et al.*, *J. Neurosci.* **41**, 2554–2565 (2021).
10. S. F. Sorrells *et al.*, *Nature* **555**, 377–381 (2018).
11. S. Cipriani *et al.*, *Cereb. Cortex* **28**, 2458–2478 (2018).
12. G. Tosoni *et al.*, *Neuron* **111**, 1714–1731.e3 (2023).
13. M. Sepp *et al.*, *Nature* **625**, 788–796 (2024).
14. Y. Zhou *et al.*, *Nature* **607**, 527–533 (2022).
15. D. Franjic *et al.*, *Neuron* **10**, P452–469.E14 (2022).
16. P. S. Eriksson *et al.*, *Nat. Med.* **4**, 1313–1317 (1998).
17. K. L. Spalding *et al.*, *Cell* **153**, 1219–1227 (2013).
18. F. Ayhan *et al.*, *Neuron* **109**, 2091–2105.e6 (2021).
19. N. Habib *et al.*, *Nat. Methods* **14**, 955–958 (2017).
20. T. Stuart *et al.*, *Cell* **177**, 1888–1902.e21 (2019).
21. Y. Hao *et al.*, *Cell* **184**, 3573–3587.e29 (2021).
22. L. McInnes, J. Healy, N. Saul, L. Großberger, *J. Open Source Softw.* **3**, 861 (2018).
23. L. Waltman, N. J. Van Eck, *Eur. Phys. J. B* **86**, 471 (2013).
24. R. D. Hodge *et al.*, *J. Neurosci.* **32**, 6275–6287 (2012).
25. V. Bergen, M. Lange, S. Peidli, F. A. Wolf, F. J. Theis, *Nat. Biotechnol.* **38**, 1408–1414 (2020).
26. P. Angerer *et al.*, *Bioinformatics* **32**, 1241–1243 (2016).
27. H. Hochgerner, A. Zeisel, P. Lönnberg, S. Linnarsson, *Nat. Neurosci.* **21**, 290–299 (2018).
28. G. La Manno *et al.*, *Cell* **167**, 566–580.e19 (2016).
29. J. Alquicira-Hernandez, A. Sathe, H. P. Ji, Q. Nguyen, J. E. Powell, *Genome Biol.* **20**, 264 (2019).
30. A. Gayoso *et al.*, *Nat. Biotechnol.* **40**, 163–166 (2022).
31. H. B. Huttner *et al.*, *Nat. Neurosci.* **17**, 801–803 (2014).
32. R. D. Bhardwaj *et al.*, *Proc. Natl. Acad. Sci. U.S.A.* **103**, 12564–12568 (2006).
33. C. Nagy *et al.*, *Nat. Neurosci.* **23**, 771–781 (2020).
34. K. Siletti *et al.*, *Science* **382**, 6667 (2023).
35. S. Zhong *et al.*, *Nature* **577**, 531–536 (2020).
36. X. Fan *et al.*, *Sci. Adv.* **6**, eaaz2978 (2020).
37. J. Andersen *et al.*, *Neuron* **83**, 1085–1097 (2014).
38. S. Jessberger, J. M. Parent, *Cold Spring Harb. Perspect. Biol.* **7**, 1–10 (2015).
39. F. Wang *et al.*, *J. Mol. Diagn.* **14**, 22–29 (2012).
40. A. Janesick *et al.*, *Nat. Commun.* **14**, 8353 (2023).
41. P. J. Lucassen, C. P. Fitzsimons, E. Salta, M. Maletić-Savatic, *Behav. Brain Res.* **381**, 112458 (2020).
42. S. B. McHugh *et al.*, *Nat. Neurosci.* **25**, 1481–1491 (2022).
43. I. Dumitru, snRNaseq_human_hippocampus, Version v1, Zenodo (2025); <https://zenodo.org/records/14879680>.
44. I. Dumitru, Xenium_1_2_3, Version v1, Zenodo (2025); <https://zenodo.org/records/14879552>.
45. I. Dumitru, Xenium_4_5_6, Version v1, Zenodo (2025); <https://zenodo.org/records/14879626>.
46. I. Dumitru, Computational Code Human Neurogenesis, Version v1, Zenodo (2025); <https://zenodo.org/records/14882965>.

ACKNOWLEDGMENTS

We thank E. Llorens-Bobadilla and J. Mold for valuable discussions. We thank N. Eckerdal, the Biostatistics Core Facility, and the Karolinska Institutet for help regarding the statistical comparisons present in the study. The tissue used in this research was obtained from the Human Brain Collection Core, Intramural Research Program, NIMH (<https://www.nimh.nih.gov/research-research-conducted-at-nimh/research-areas/research-support-services/hbcc>). Human tissue was also received from KI Donatum, the NIH NeuroBioBank at the University of Maryland, the University of Miami, and from the Medical Research Council Biobank in UK, from King's College London. The authors acknowledge the In Situ Sequencing Facility at SciLifeLab, funded by Science for Life Laboratory; the authors also acknowledge the Swedish Research Council for providing in situ sequencing services. **Funding:** This work was funded by the following: The Swedish Research Council, ERC (ERC-2015-AdG-695096) (to J.F.); the Swedish Cancer Foundation (to J.F.); Knut och Alice Wallenbergs Stiftelse (to J.F.); The Swedish Society for Strategic Research and the Strategic Research Programme in Stem Cells and Regenerative Medicine at Karolinska Institutet (StratRegen) (to J.F.); the EMBO long term fellowship and a Marie Skłodowska-Curie Action (to I.D.); and the Knut and Alice Wallenberg Foundation as part of the National Bioinformatics Infrastructure Sweden at SciLifeLab (to Å.B. and R.S.). **Author contributions:** Conceptualization and methodology: I.D., J.F., M.P., M.Z., C.Z., and R.S. Methodology: I.D., J.F., M.P., M.Z., C.Z., K.A., H.D., R.S., and S.G. Primary analysis: I.D. and C.Z. Secondary analysis: I.D., M.Z., and C.Z. Visualization: I.D., M.Z., C.Z., and M.P.; Funding acquisition: J.F. Project administration: I.D. and J.F. Writing – original draft: I.D. Writing – review & editing: I.D. and J.F. and all authors; Supervision: J.F. and R.S. **Competing interests:** J.F. and M.Z. are consultants to 10x Genomics. I.D. started working at AAX Biotech AB in December 2024. C.Z. has been the CEO of Xpress genomics since 2022. **Data and materials availability:** All sequencing data in the study and the Xenium data are freely available and are deposited at Zenodo: snRNA-seq dataset (43) and Xenium datasets (44) and (45). The computational code used in this study is available at Zenodo (46). The raw FASTQ files have been deposited in the European Nucleotide Archive (ENA) under study accession number ERP173468. **License information:** Copyright © 2025 the authors, some rights reserved; exclusive licensee American Association for the Advancement of Science. No claim to original US government works. <https://www.science.org/content/page/science-licenses-journal-article-reuse>

SUPPLEMENTARY MATERIALS

science.org/doi/10.1126/science.adu9575
Materials and Methods; Figs. S1 to S26; Tables S1 and S2; References (47–56); MDAR Reproducibility Checklist

Submitted 28 November 2024; accepted 25 April 2025

10.1126/science.adu9575